

VARIATION OF EMITTIVITY WITH POWDER BED FUSION BUILD PARAMETERS

J. C. Heigel*, B. M. Lane*, and S. P. Moylan*

*National Institute of Standards and Technology¹, Gaithersburg, MD 20899

Abstract

Common approaches to process monitoring of powder bed fusion rely heavily on optical measurements. These measurements can be used to verify powder spreading, assess the quality of each layer, and measure process temperatures. In regards to the latter, radiometric detectors such as cameras or pyrometers only measure radiant emissions from the surface, and do not directly measure its temperature. Calculating the temperature from these measurements relies on the calibration of the camera or pyrometer with a blackbody and on knowledge of the emittivity of the surface being measured. Emittivity depends on multiple factors including surface texture and viewing angle, among others. An apparatus and method for measuring emittivity using an infrared camera is detailed. Measured emittivity values from metal surfaces produced using a commercial powder bed fusion process are presented and related to temperature, viewing angle, and oxidation state.

Introduction

The outcome of a metal part produced with additive manufacturing (AM) is dependent on the thermal history of the part. For instance, it has been shown that the microstructure grows in the direction of the material deposition, and the characteristics of the microstructure is dependent on the cooling rates [1]. The residual stress has also been shown to be sensitive to the thermal history, as well as how a specific material's microstructure responds to that history [2]. Although the thermal history can be simulated using finite element analysis [3], which can in turn be used to predict the microstructure [4], residual stress and distortion [5], and even the melt pool geometry [6], accurate temperature measurement during AM processes is necessary to validate these models and to monitor the process for part certification [7].

The temperature during an AM build can be measured using either direct contact methods, such as thermocouples, or optical methods, such as pyrometers or thermal cameras. Although thermocouples can accurately measure temperature and have been used to study AM processes [2] and to validate models [5], their use for AM processes is limited. Specifically, they must be preplaced on a substrate and cannot be used to measure the temperature of newly added part layers. Builds have been paused to attach thermocouples to newly formed layers to study the process after it is resumed [5, 8], but this approach cannot be used to qualify parts because the pause allows the part to cool more between layers and it has been shown that changing the time between layers can significantly affect the microstructure and material properties of the final part [9].

¹ Certain commercial equipment, instruments, or materials are identified in this paper in order to specify the experimental procedure adequately. Such identification is not intended to imply recommendation or endorsement by the National Institute of Standards and Technology, nor is it intended to imply that the materials or equipment identified are necessarily the best available for the purpose. This publication was prepared by United States Government employees as part of their official duties and is, therefore, a work of the U.S. Government and not subject to copyright.

Pyrometers and infrared cameras are attractive alternatives to thermocouples for monitoring AM processes because they can measure the radiation of each newly formed layer which can in turn be used to calculate the temperature. For instance, a high speed (2 031 frames/s) infrared camera was used to study the highly dynamic AM process and the particles that are ejected from the melt pool [10]. At the National Institute of Standards and Technology (NIST), a thermography setup has been developed to study the size of the melt pool and the cooling rates of the material around it [11]. However, an accurate calculation of the temperature from these thermographic measurements relies on a thorough understanding of the emissivity of the newly produced part surface.

Emissivity is a non-dimensional value between 0 and 1 that relates the emission of a surface to that of a perfectly emitting black body. Although the term emissivity is commonly used in the literature instead of emittivity, each term refers to a different effect. Emissivity is a property of a material, while emittivity is a property of a surface. Emittivity, which is inherently sensitive to the texture of a surface, has also been shown in the literature to vary based on temperature and viewing angle [12]. Unfortunately, there is no literature documenting the emittivity of surfaces created using AM.

The objective of this work is to demonstrate a method to determine the emittivity of AM metal part surfaces and to present some preliminary findings. The method utilizes a copper fixture and cartridge heaters to hold and heat AM produced samples to high uniform temperatures, while a thermal camera measures the infrared emissions from the top surface of the sample. The emittivity is then calculated from the camera signal and direct measurements of the sample acquired using thermocouples. Samples are produced using different processing conditions that result in varying surface textures to understand their effect on emittivity. In addition, the sensitivity of emittivity to the viewing angle and deposition track orientation is investigated.

Experimental Method

Emittivity (ε) cannot be directly measured, but is instead calculated by relating the measured infrared camera signal (S_{meas}) to measurements of the actual temperature of that surface (T_{true}) and of the ambient environment (T_{amb}). The relationship between these values is defined by the measurement equation, which is a model representing the total radiation collected by the camera:

$$F(S_{meas}) = \varepsilon \cdot F(T_{true}) + (1 - \varepsilon) \cdot F(T_{amb}) \quad (1)$$

Equation (1) assumes that the total radiation measured by the camera consists of radiation emitted from the sample surface, represented by $\varepsilon \cdot F(T_{true})$, and reflected radiation from the surroundings, represented by $(1 - \varepsilon) \cdot F(T_{amb})$. The functions $F(T_{true})$ and $F(T_{amb})$ are derived from Planck's law [13]. The function $F(S_{meas})$ relates the camera signal to the radiant temperature of a target and ultimately the collected electromagnetic radiation. A blackbody calibration is used to develop $F(S_{meas})$ [11].

Two considerations must be noted when using the above relationship to calculate emittivity. First, under certain circumstances, T_{amb} does not necessarily equate to the ambient temperature of the surroundings, but can be used as a correction factor to account for reflected radiation. Second, ε is used as a 'correction factor' for converting thermal camera measurements to temperature, and will depend on the specific camera, filter, optics, and other factors. However, temperature and angular dependence of this emittivity factor are physically relatable to measurements made.

Figure 1 shows the setup used, which enables a sample to be mounted in a copper block that is heated by two cartridge heaters. Finite element modeling was used to determine an

appropriate location for the sample with respect to the cartridge heaters to ensure a surface temperature deviation of less than 2 °C. The sample is heated to a desired temperature so that it can be imaged by an infrared camera. Nickel alloy (IN 625) samples are created in a commercial powder bed fusion (PBF) machine. The top surface of each 3.18 mm thick sample measures 8.33 mm long and 5.09 mm wide. Two thermocouples are then welded to the top surface, each on opposing sides. One of the thermocouples is used as an input for the proportional-integral-derivative (PID) controller that controls the heater while the other is used to measure the surface temperature of the sample and is recorded by a data acquisition device. The average temperature calculated from these two thermocouples is assumed to be the temperature across the entire top surface of the sample (T_{true}). Once the thermocouples are attached, the sample is placed inside a cavity in the copper block and then an IN 625 plate, which is also produced using the same AM process, is bolted to the base to hold the sample firmly in position, ensuring the best heat transfer between the sample and the copper block. Two cartridge heaters, which are controlled by the PID controller, are placed inside two holes in the copper block. These are capable of heating the sample to just over 500 °C.

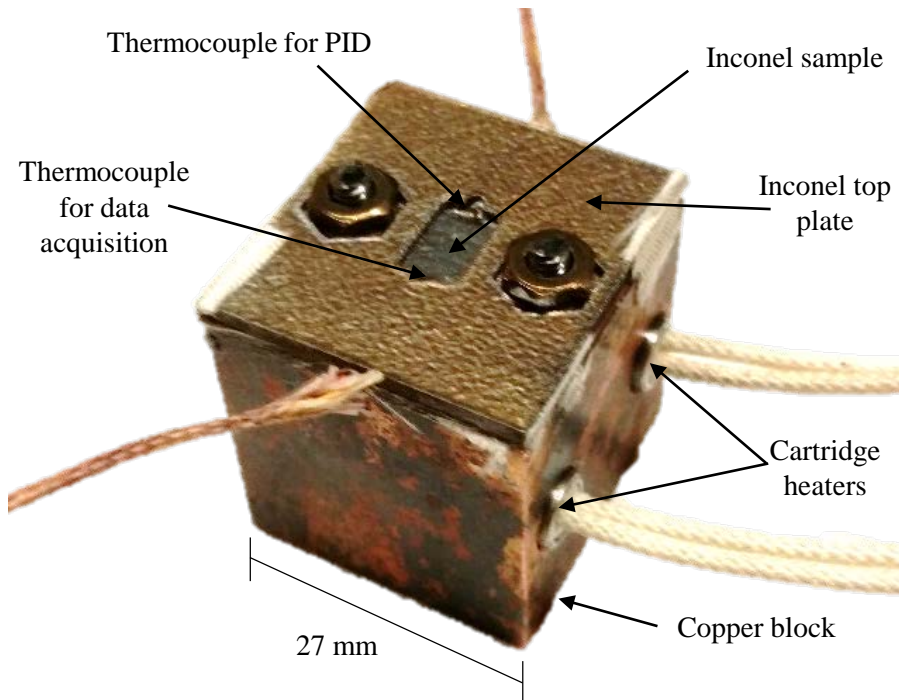


Figure 1 – A PBF produced sample inside of the PID controlled heater.

Table 1 presents the processing conditions used to create the four different samples used in this study. Each sample is produced during the same build in the middle of the build plate. The hatch spacing and layer thickness for each sample are the same, and the scan direction of all layers is consistent (no relative rotation between layers). The difference between samples lies in the laser power and scan speed used to fuse the IN 625 powder, as well as the post-process treatment of each sample. Samples 1 and 3 are produced using a laser power of 195 W scanning at a speed of 800 mm/s. These are the manufacturer recommended values for this material. Samples 2 and 4 are created using a power and speed that is only a quarter of those values, which was shown to also produce acceptable tracks [14]. For the current study, samples produced with a slower scan speed are desirable because future thermography work would benefit from slower

speeds because more data can be collected with the same camera frame rate. After the PBF process and before the measurements are taken to calculate emittivity, Samples 1 and 2 are held at a temperature of 500 °C for approximately 2 h in the ambient atmosphere. This is done to allow them to oxidize so that measurements can be performed easily without the surface changing due to oxidation.

Table 1 – PBF processing conditions used to create each of the four samples.

Sample #	Laser power (W)	Scan speed (mm/s)	Scan direction of all layers	Hatch spacing (μm)	Layer thickness (μm)	Post-process oxidation
1	195	800	X-axis	100	20	Yes
2	49	200	X-axis	100	20	Yes
3	195	800	X-axis	100	20	No
4	49	200	X-axis	100	20	No

Figure 2 shows the measurement setup used to determine the emittivity of each sample. The copper base with a sample mounted in it is placed inside the cavity of a fire brick to minimize its heat loss. The fire brick is then placed into a rig that allows the relative angle between the sample and an infrared camera to be changed. This is done to investigate the impact of viewing angle on the infrared measurement. Infrared measurements are then performed using the same camera and optics implemented by Lane et al. [11]. Consequently, the results reported in the current study are only directly applicable to that work, however the reported trends are expected to be broadly applicable.

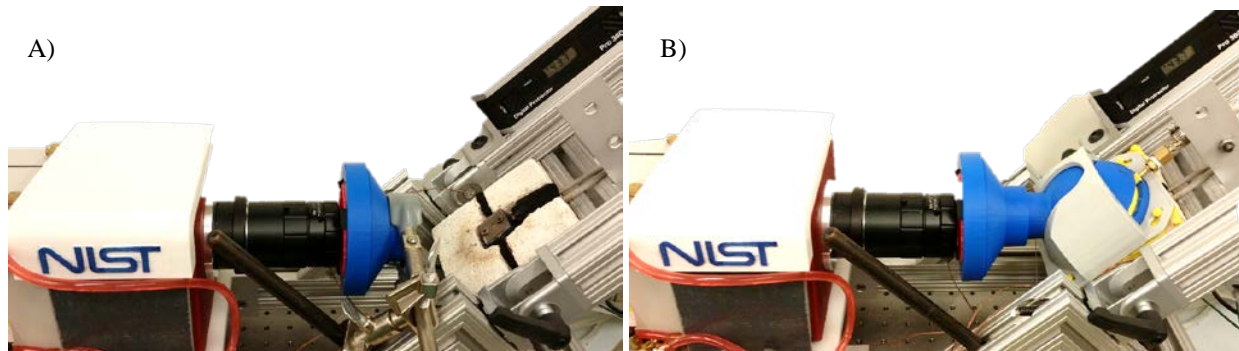


Figure 2 – The measurement setup. A) Shows the setup used to measure Samples 1 & 2, which are first allowed to oxidize. B) shows the setup used to measure Samples 3 & 4, where a dome is placed over the sample and nitrogen gas is supplied to displace oxygen and prevent oxidation at the elevated temperatures.

To replicate the setup used in the earlier study [11], a piece of glass used in the custom viewing door is located between the sample and the infrared camera. The infrared camera measures the emissions from the samples at a frame rate of 60 Hz and an integration time of 200 ms. A filter is included in the optical system to restrict the detectable wavelengths to a range between 1350 nm and 1600 nm. Although the frame rate and integration time is lower than those described in [11], these differences do not affect the determination of emittivity since the measured signal value S_{meas} , and the calibration function $F(S_{meas})$ both scale with integration time

in Equation (1), and the spectral bandwidth (filter) is the same. It also allows for a lower measureable temperature range, which is encountered with the current sample heater.

Results

The difference in processing conditions and post-process oxidation is apparent to the naked eye, as shown in Figure 3, which presents images obtained with a visible light microscope. In these images, the surface was generated with the laser scanning parallel to the X axis, starting along the top edge and alternating directions until it completed at the bottom edge. Comparisons between these images reveal that the samples produced with the higher laser power and faster scan speed, Samples 1 and 3, appear to have a smoother surface than those produced with the lower power and slower speed, Samples 2 and 4. That is, the individual tracks, which appear as horizontal lines in these images, are more pronounced in Samples 2 and 4. In addition, it appears that the oxidation of Samples 1 and 2 changes their color, making them appear more brown and blue compared to their non-oxidized counterparts.

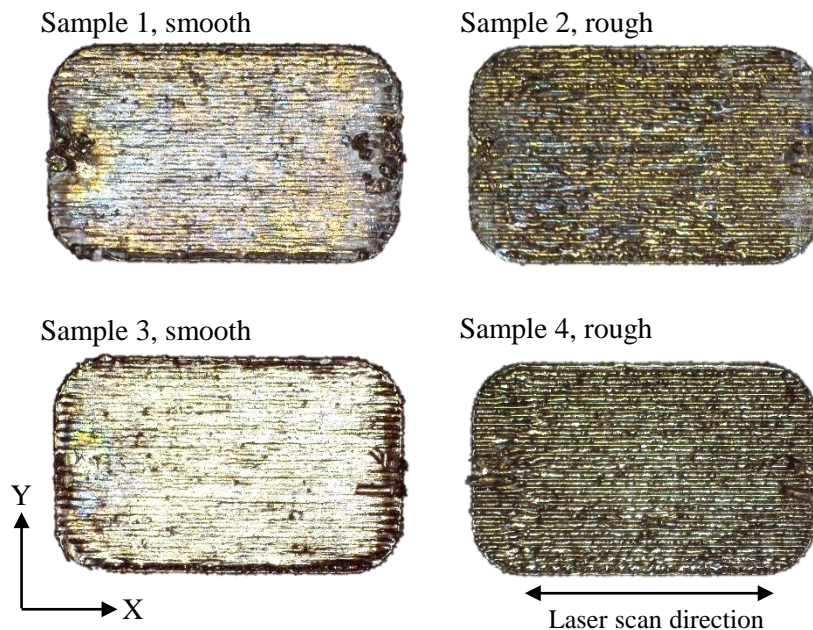


Figure 3 – Images of the top surface of each 8.33 mm wide, 5.09 mm tall sample.
Sample 1 – 195 W, 800 mm/s, oxidized. Sample 2 – 49 W, 200 mm/s, oxidized.
Sample 3 – 195 W, 800 mm/s, not oxidized. Sample 4 – 49 W, 200 mm/s, not oxidized.

In order to verify the perceived differences in surface roughness, the surfaces of Samples 1 and 2 are measured using a scanning white light interferometer. Figure 4 shows the 3-dimensional results and confirms that the individual scan tracks are more pronounced in Sample 2, which uses the lower laser power and slower scan speed. In addition to providing qualitative assessment of the difference between these two surfaces, roughness statistics are calculated to provide a quantitative comparison. This analysis is performed within the analysis region indicated in each image in Figure 4.

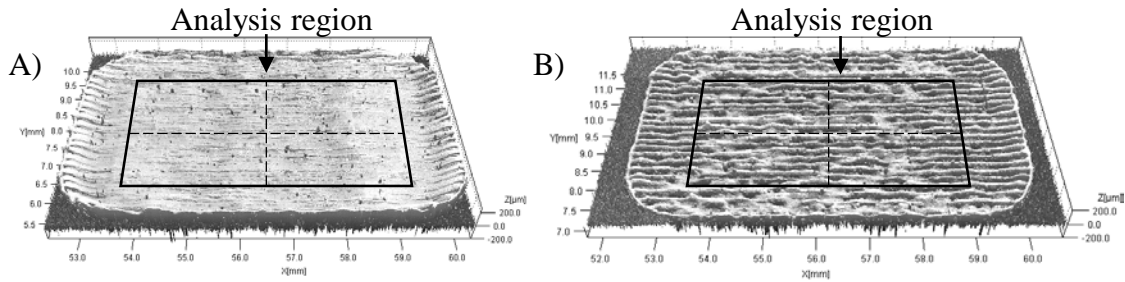


Figure 4 – Images of the top surface of two different samples obtained using a scanning white light interferometer, and analysis region in which roughness data is calculated
 A) Sample 1 produced using a laser power of 195 W and scanning speed of 800 mm/s.
 B) Sample 2 produced using a laser power of 49 W and a scanning speed of 200 mm/s.

Table 2 presents the roughness statistics calculated from the scanning white light interferometer measurements of Samples 1 and 2. Roughness is calculated using a variety of methods. The arithmetic mean deviation (Ra), root mean square deviation (Rq), mean height of the profile elements (Rc), and the skewness (Rsk) are calculated according to method described by ISO 4287 [15]. These values are calculated along a line parallel to the laser scan tracks (subscript X) and perpendicular to the tracks (subscript Y). The locations of these lines are indicated by the dashed lines in Figure 4. In addition, the area roughness average (Sa), area root mean square (Sq), and the area skewness (Ssk) are calculated using all of the data within the analysis region indicated in Figure 4.

Table 2 – Surface roughness statistics.

Sample #	Parallel roughness				Perpendicular roughness				Area roughness		
	Ra_x μm	Rq_x μm	Rc_x μm	Rsk_x	Ra_y μm	Rq_y μm	Rc_y μm	Rsk_y	Sa μm	Sq μm	Ssk
1	0.21	0.27	0.77	-0.410	1.48	2.36	8.01	0.923	11.79	14.57	-0.25
2	0.25	0.31	0.82	-0.36	3.28	4.84	11.88	-0.313	27.18	32.28	0.03

The values presented in Table 2 show that by all measures the lower power and slower speed used to produce Sample 2 result in a rougher surface than the higher power and faster speed used to create Sample 1. Preliminary measurements indicate that the roughness of Samples 3 and 4 are similar to Samples 1 and 2, respectively. From these results, it is theorized that Samples 2 and 4 will have higher emittivity compared to Samples 1 and 3, since the literature has shown that rougher surfaces tend to result in higher emittivity values [12]. The following results and analysis confirm this theory.

Figure 5 presents images of Samples 1 and 2 acquired using the infrared camera. In each image, the sample is oriented horizontally such that the tracks appear to go left to right, similar to the images presented in Figure 3 and Figure 4. The IN 625 top plate, which holds the sample in the copper cube, can be seen along the edges. On the sides of each sample, approximately half-way up, two thermocouples can be seen welded to the surface. A white box identifies the analysis region.

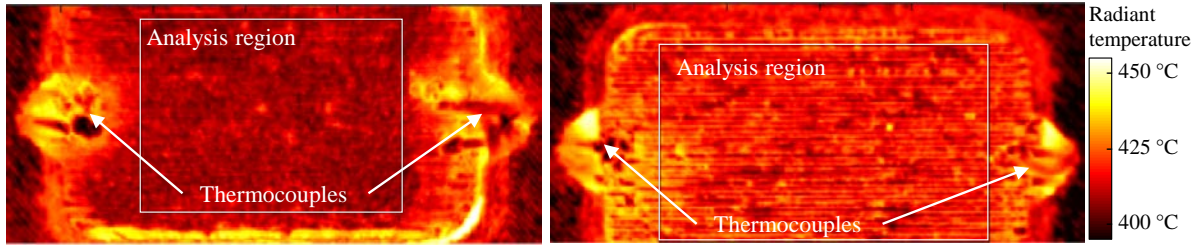


Figure 5 – Images from the infrared camera. Each image is taken with the surface perpendicular to the line of sight (90°). A) shows the smooth surface of Sample 1 (195 W, 800 mm/s). B) shows the rough surface of Sample 2 (49 W, 200 mm/s). Each image uses the same scale (radiant temperature °C).

Two observations can be made from these images. First, the radiant temperature across each sample is relatively uniform apart from local variations due to surface texture, indicating a uniformly heated sample. The second observation is that Sample 2 emits more than Sample 1. For instance, although each sample is at the same temperature of 450 °C, the smooth surface of Sample 1 appears to be $413 \text{ °C} \pm 2 \text{ °C}$ while the rough surface of Sample 2 appears to be hotter $421 \text{ °C} \pm 5 \text{ °C}$ within the analysis region. This difference in radiant temperature is attributed to difference in emittivity of the two PBF surfaces.

Figure 6 presents the emittivity of each sample at a variety of temperatures. In this figure, the emittivity is calculated from measurements made when the top surface of the sample is perpendicular to the camera’s line of sight. There are several observations that can be made from this data. First, as noted earlier, samples produced with the higher laser power speed (Samples 1 and 3), which have smoother surfaces, have lower emittivity than those produced with lower powers and speeds (Samples 2 and 4). For example, at 500 °C, Sample 1 has an emittivity of 0.680 while Sample 2 has an emittivity of 0.761, a difference of 12 %.

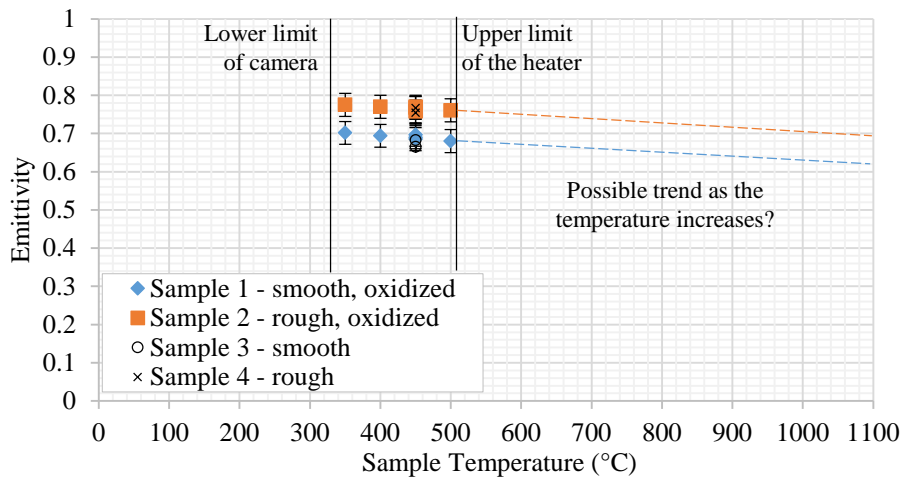


Figure 6 – Emittivity vs. sample temperature. The dashed lines represent a theoretical extrapolation of the data to higher temperature. There is no data presented to support these trends, they only illustrate a possible trend. Uncertainty bars represent 1 standard deviation.

The second observation is that there is little difference between oxidized and non-oxidized samples produced with the same processing conditions. Although further analysis is needed to support this finding, these preliminary results indicate that for the extent that Samples 1 and 2 are oxidized, it has no significant effect on emittivity for the wavelength range measured in this study.

This is fortunate since keeping the sample in a controlled environment adds a layer of complexity to emittivity measurements. If the oxide layer does not significantly affect the emittivity, then it can be determined much easier in an ex-situ measurement apparatus. However, further work is required to verify this observation, and it is unlikely that this will be the case for other metal alloys.

The third observation is that the data presented in Figure 6 suggests that emittivity gradually decrease as the sample temperature rises. However, the literature for other nickel alloys indicates that emittivity remains fairly constant over a similar temperature range [12]. Therefore, a more detailed investigation is necessary to understand the relationship between temperature and emittivity of IN 625 before any conclusions can be drawn.

The results presented in Figure 7 and Figure 8 indicate that the sensitivity of emittivity to viewing angle is dependent on surface roughness, which is sensitive to both processing conditions and scan track orientation. When rotating the sample about the X axis, Figure 7 demonstrates that the emittivity of Sample 1, which has lower roughness statistics, increases by 10 % as the viewing angle becomes more acute, while the emittivity of Sample 2 only varies by 2 %. However, when rotating about the Y axis (Figure 8), the emittivity of Sample 1 increases by only 3 % while the emittivity of Sample varies by only 1 %. Considering these results, it is important to not only account for the surface roughness resulting from different processing conditions, but also the orientation of the infrared camera/sensor and the track orientation.

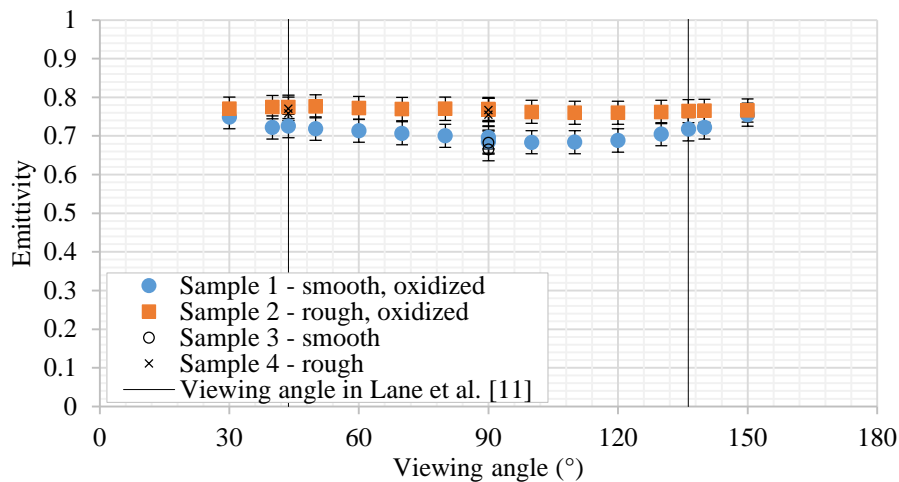


Figure 7 – Emittivity vs. viewing angle by rotating the sample about the X-axis shown in Figure 3. The sample temperature is 450 °C. Uncertainty bars represent 1 standard deviation.

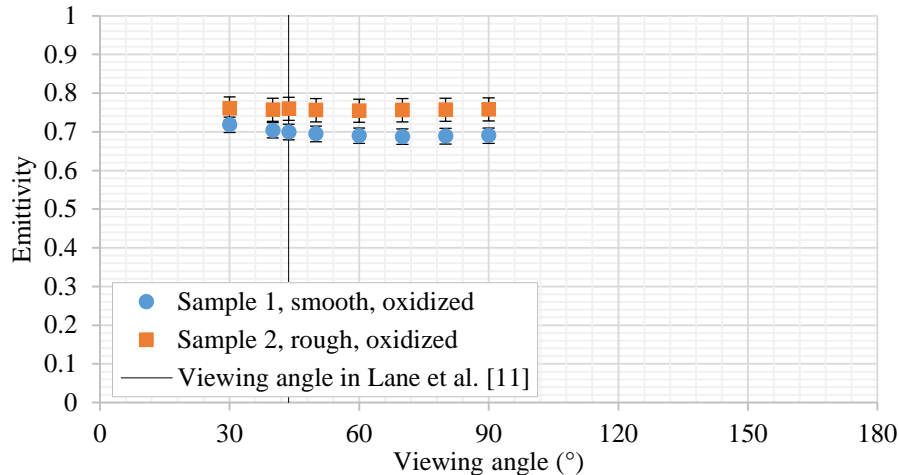


Figure 8 – Emittivity vs. viewing angle by rotating the sample about the Y-axis shown in Figure 3. The sample temperature is 450 °C. Uncertainty bars represent 1 standard deviation. The measurement setup prohibited rotation about the Y-axis between 90° and 150°.

Conclusions

An investigation into the surface averaged emittivity, filtered at 1350 nm to 1600 nm, of IN 625 surfaces produced using different PBF processing conditions was presented. The emittivity was calculated from infrared measurements of samples heated in a controlled, uniform manner. The preliminary results presented in this work indicate the following:

- 1) The laser power and scan speed used to create PBF parts can significantly affect the surface characteristics and resulting emittivity of the surface. In the cases investigated a 12 % difference was observed.
- 2) Emittivity is sensitive to the viewing angle, but the extent is dependent on the surface roughness that results from different processing conditions. The emittivity of the rougher samples in this study varied by 2 % over a wide viewing angle range, whereas the smoother samples varied by 10 % over the same range.
- 3) The orientation of the deposition tracks affects the sensitivity of emittivity to viewing angle.
- 4) Oxidation of the IN 625 in this study negligibly affected emittivity.

Although the findings presented in this work can inform the design of an infrared imaging system for a PBF process and the analysis of the acquired data, care should be exercised because these values are specific to the measurement setup. It is possible that the reported emittivity values could change if different optical elements, such as filters, are used. However, the reported trends are expected to be consistent. Therefore, it is advisable to repeat these or similar measurements to acquire the appropriate emittivity values for the chosen system.

References

- [1] S. M. Kelly and S. L. Kampe, “Microstructural evolution in laser-deposited multilayer Ti-6Al-4V builds: Part I. Microstructural characterization,” *Metallurgical and Materials Transactions A*, vol. 35, no. 6, pp. 1861–1867, 2004.
- [2] E. R. Denlinger, J. C. Heigel, P. Michaleris, and T. A. Palmer, “Effect of inter-layer dwell time on distortion and residual stress in additive manufacturing of titanium and nickel alloys,” *Journal of Materials Processing Technology*, vol. 215, pp. 123–131, Jan. 2015.

- [3] P. Michaleris, "Modeling metal deposition in heat transfer analyses of additive manufacturing processes," *Finite Elements in Analysis and Design*, vol. 86, no. 1, pp. 51–60, 2014.
- [4] J. Irwin, E. W. Reutzel, P. Michaleris, J. Keist, and A. R. Nassar, "Predicting microstructure from thermal history during additive manufacturing for Ti-6Al-4V," *Journal of Manufacturing Science and Engineering*, vol. 138, 2016.
- [5] J. C. Heigel, P. Michaleris, and E. W. Reutzel, "Thermo-mechanical model development and validation of directed energy deposition additive manufacturing of Ti-6Al-4V," *Additive Manufacturing*, vol. 5, pp. 9–19, 2015.
- [6] L. Han, F. W. Liou, and S. Musti, "Thermal behavior and geometry model of melt pool in laser material process," *Journal of Heat Transfer*, vol. 127, pp. 1005–1014, 2005.
- [7] Energetics Inc. for National Institute of Standards and Technology, "Measurement science roadmap for metal based additive manufacturing," May 2013.
- [8] M. L. Griffith, M. E. Schlienger, L. D. Harwell, M. T. Ensz, D. L. Greene, J. E. Smugeresky, C. V. Robino, W. H. Hofmeister, M. J. Wert, and D. V. Nelson, "Understanding thermal behavior in LENS processing of structural materials," Sandia Corporation, SAND098-2475C, 1998.
- [9] A. Yadollahi, N. Shamsaei, S. M. Thompson, and D. W. Seely, "Effects of process time interval and heat treatment on the mechanical and microstructural properties of direct laser deposited 316L stainless steel," *Materials Science and Engineering: A*, vol. 644, pp. 171–183, Sep. 2015.
- [10] F. Bayle and M. Doubenskaia, "Selective laser melting process monitoring with high speed infra-red camera and pyrometer," in *SPIE Proceedings*, 2008.
- [11] B. Lane, S. Moylan, E. Whinton, and L. Ma, "Thermographic Measurements of the Commercial Laser Powder Bed Fusion Process at NIST," in *Solid Freeform Fabrication Symposium*, Austin, TX, 2015, p. 575.
- [12] L. del Campo, R. B. Pérez-Sáez, L. González-Fernández, X. Esquisabel, I. Fernández, P. González-Martín, and M. J. Tello, "Emissivity measurements on aeronautical alloys," *Journal of Alloys and Compounds*, vol. 489, no. 2, pp. 482–487, Jan. 2010.
- [13] B. Lane, E. Whinton, V. Madhavan, and A. Donmez, "Uncertainty of temperature measurements by infrared thermography for metal cutting applications," *Metrologia*, vol. 50, no. 6, p. 637, 2013.
- [14] C. Montgomery, J. Beuth, L. Sheridan, and N. Klinbeil, "Process mapping of Inconel 625 in laser powder bed additive manufacturing," presented at the Solid Freeform Fabrication Symposium, Austin, TX, 2015, pp. 1195–1204.
- [15] "ISO 4287:1997 - Geometrical Product Specifications (GPS) -- Surface texture: Profile method -- Terms, definitions and surface texture parameters," *ISO*. [Online]. Available: http://www.iso.org/iso/catalogue_detail.htm?csnumber=10132. [Accessed: 29-Aug-2016].